Molecular Therapy
Original Article

Innate Inhibiting Proteins Enhance Expression and Immunogenicity of Self-Amplifying RNA

Anna K. Blakney,[1] Paul F. McKay,[1] Clément R. Bouton,[1] Kai Hu,[1] Karnyart Samnuan,[1] and Robin J. Shattock[1]

[1]Department of Infectious Disease, Imperial College London, London W21PG, UK

Self-amplifying RNA (saRNA) is a cutting-edge platform for both nucleic acid vaccines and therapeutics. saRNA is self-adjuvanting, as it activates types I and III interferon (IFN), which enhances the immunogenicity of RNA vaccines but can also lead to inhibition of translation. In this study, we screened a library of saRNA constructs with *cis*-encoded innate inhibiting proteins (IIPs) and determined the effect on protein expression and immunogenicity. We observed that the PIV-5 V and Middle East respiratory syndrome coronavirus (MERS-CoV) ORF4a proteins enhance protein expression 100- to 500-fold *in vitro* in IFN-competent HeLa and MRC5 cells. We found that the MERS-CoV ORF4a protein partially abates dose nonlinearity *in vivo*, and that ruxolitinib, a potent Janus kinase (JAK)/signal transducer and activator of transcription (STAT) inhibitor, but not the IIPs, enhances protein expression of saRNA *in vivo*. Both the PIV-5 V and MERS-CoV ORF4a proteins were found to enhance the percentage of resident cells in human skin explants expressing saRNA and completely rescued dose nonlinearity of saRNA. Finally, we observed that the MERS-CoV ORF4a increased the rabies virus (*RABV*)-specific immunoglobulin G (IgG) titer and neutralization half-maximal inhibitory concentration (IC_{50}) by ~10-fold in rabbits, but not in mice or rats. These experiments provide a proof of concept that IIPs can be directly encoded into saRNA vectors and effectively abate the nonlinear dose dependency and enhance immunogenicity.

INTRODUCTION

Self-amplifying RNA (saRNA) is a highly advantageous platform for both nucleic acid vaccines and therapeutics. Derived from an alphavirus genome,[1] saRNA encodes the alphaviral replicase and a gene of interest (GOI), which replaces the structural proteins of the virus. A variety of GOIs have been incorporated and shown to be highly immunogenic with the saRNA platform, including vaccine antigens for influenza,[2] HIV-1,[3,4] respiratory syncytial virus (RSV),[3,5] and Ebola.[6] Furthermore, saRNA vaccines are rapidly scalable, as they require a minimal dose compared to messenger RNA (mRNA),[7] which is highly useful in the context of both normal vaccine production but also global pandemics. saRNA is self-adjuvanting,[8] as it activates a type I interferon (IFN) through endosomal sensing via Toll-like receptor (TLR)3, TLR7, and TLR8 as well as cytosolic sensing via melanoma differentiation-associated protein 5 (MDA5), retinoic acid-inducible gene I (RIG-I), protein kinase R (PKR), 2′-5′-oligoadenylate synthetase (OAS), as well as other possibly unknown pathways.[9]

While self-adjuvantation is advantageous and enhances the immunogenicity of RNA vaccines, this phenomenon is a double-edged sword, as innate recognition of mRNA upregulates the expression and activation of PKR and OAS, which leads to the inhibition of translation[10] and degradation of cellular mRNA.[11] Increasing doses of RNA are correlated with an increase of injection site reactions as well as systemic adverse events in human patients,[12] which are likely due to the innate immune response to RNA. Furthermore, there is a disparity between the immunogenicity of RNA vaccines in preclinical animal models and human clinical trials, wherein RNA formulations are highly potent in lower order animal species such as mice, ferrets, and even nonhuman primates, but exhibit orders of magnitude lower potency in humans.[12] This is likely due to inherent differences in innate immunity between different species, such as transcriptionally diverging genes that encode cytokines and chemokines.[13]

Innate immune sensing is especially critical for saRNA, as the self-replication leads to an exponential increase in copies of RNA in the cytoplasm as well as double-stranded RNA (dsRNA) intermediates.[14,15] One potential strategy to reduce detrimental effects of type I IFN activation on RNA vaccines is to encode innate inhibiting proteins (IIPs) directly in the RNA, similar to the mechanism by which RNA viruses evade innate immune recognition and dampen the IFN response.[16] Liu et al.[17] observed that co-transfection of the E3, K3, and B18R (EKB) protein of vaccinia virus and non-structural protein 1 (NS1) of influenza A virus enhanced translation of mRNA. Beissert et al.[18] similarly observed enhanced protein expression *in vitro* and *in vivo* with the EKB proteins encoded by mRNA. However, this approach requires administration of two different types of RNA and does not guarantee co-localization of the IIP in the same cell as the GOI mRNA, which is imperative for overcoming innate sensing.

In this study, we screened a library of saRNA constructs with *cis*-encoded IIPs and determined the effect on protein expression and

Received 17 June 2020; accepted 5 November 2020;
https://doi.org/10.1016/j.ymthe.2020.11.011.

Correspondence: Anna K. Blakney, Department of Infectious Disease, Imperial College London, London W21PG, UK.
E-mail: a.blakney@imperial.ac.uk
Correspondence: Robin J. Shattock, Department of Infectious Disease, Imperial College London, London W21PG, UK.
E-mail: r.shattock@imperial.ac.uk

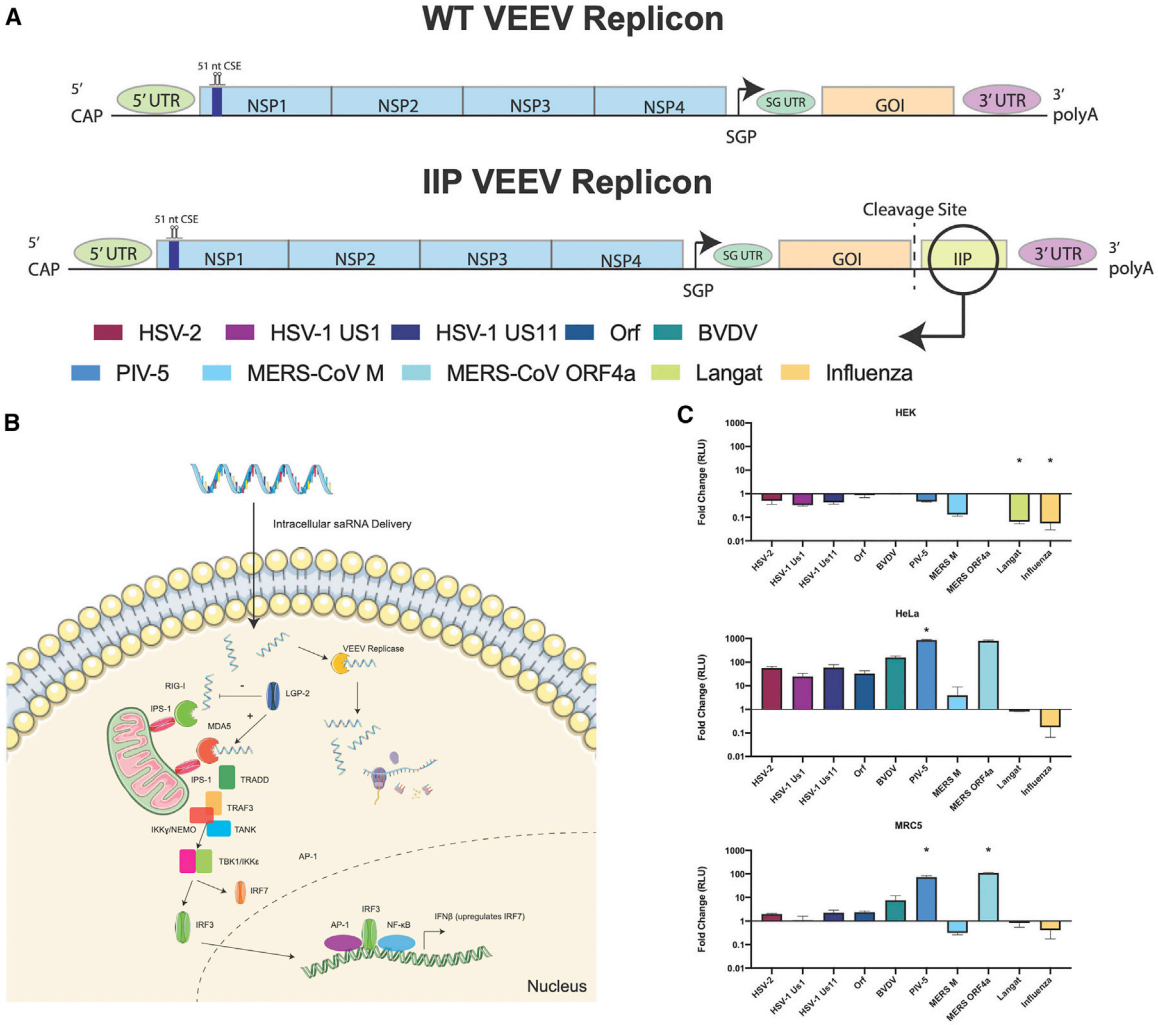

Figure 1. Schematic and *In Vitro* Protein Expression from WT and IIP VEEV Replicons

(A) Schematic of wild-type and *cis*-encoding IIP VEEV replicons. (B) Schematic of innate sensing of self-amplifying RNA. (C) *In vitro* transfection of firefly luciferase saRNA in HEK293T.17, HeLa, and MRC5 cells measured as relative light units (RLU). Bars represent mean fold change ± standard deviation normalized to wild-type VEEV control, for n = 3.

immunogenicity. We chose a range of IIPs based on their varied targets in the type I IFN pathway (Figure 1; Table 1), including the herpes simplex virus 2 (HSV-2) US1,[19] herpes simplex virus 1 (HSV-1) US1 and US11,[20,21] Orf virus OV20.0L,[22,23] bovine viral diarrhea virus (BVDV) Npro,[24,25] parainfluenza virus 5 (PIV-5) V,[26,27] Middle East respiratory syndrome coronavirus (MERS CoV) M,[28–30] and ORF4a,[31,32] Langat virus NS5,[33,34] and influenza virus NS1 proteins.[35] We characterized the library of saRNA IIP constructs *in vitro* in mouse, rabbit, nonhuman primate, and human cells with varying IFN competencies, as well as *in vivo* for both intracellular and secreted protein expression. Furthermore, we characterized how co-formulation with ruxolitinib, a potent US Food and Drug Administration (FDA)-approved Janus kinase (JAK)/signal transducer and activator of transcription (STAT) inhibitor,[36] affects protein expression *in vivo* in mice and *ex vivo* in human skin explants. We characterized the immunogenicity of IIP saRNA encoding the rabies virus (*RABV*) glycoprotein in mice, rats, and rabbits, including antibody titers and viral neutralization. Finally, we characterized activation of IFN regulatory factor 3 (IRF3) and nuclear factor κB (NF-κB) transcription factors and cytokine responses in response to wild-type (WT) and IIP saRNA.

RESULTS

IIPs Enhance Protein Expression of saRNA *In Vitro*

We first sought to determine whether the library of IIPs enhanced firefly luciferase (*fLuc*) protein expression *in vitro*. We prepared a library of saRNA VEEV replicons with an IIP separated from the *fLuc* with a T2A cleavage site (Figure 1A), with a variety of cytoplasmic

Table 1. Innate Inhibiting VEEV Replicons and Associated IFN Targets

Construct	Pathway Target
HSV-2 Us1	inhibits IFN-B production by suppressing association of IRF3 with IFN-β promoter
HSV-1 Us1	control
HSV-1Us11	binds to PACT and blocks MDA5 and RIG-I signaling
Orf OV20.0L	binds to dsRNA and inhibits both PKR and PACT, blocking RIG-I signaling
BVDV Npro	blocks IRF3 phosphorylation
PIV-5 V	blocks MDA5 and IRF3 by binding to MDA5
MERS-CoV M	interacts with TRAF3 and disrupts TRAF3-TBK1 association leading to reduced IRF3 activation
MERS-CoV ORF4a	binds to dsRNA with a preference for long RNA and suppressed PACT triggering of MDA5 and RIG-I
Langat NS5	downregulates IFNA1R and impairs JAK/STAT signaling
Influenza NS1	binds to dsRNA and blocks RIG-I signaling

IFN targets (Table 1), including IRF3, MDA5, RIG-I, and JAK/STAT (Figure 1B). We then transfected the saRNA into HEK293T.17, HeLa, and MRC5 cells using pABOL (Figure 1C; Figure S1), a polymeric delivery system that has previously been characterized to yield relatively high protein expression but is relatively immune silent due to its bioreducible nature.[2] We chose these three cell lines for their variation in completeness of the IFN pathway; HEK293T.17 cells do not have a complete pathway, as they lack endogenous RIG-I and MDA5 expression,[37,38] and thus should be less sensitive to proteins affecting this pathway, whereas HeLa and MRC5 cells are more discriminatory.[39,40] We observed that none of the IIP replicons enhanced protein expression in HEK293T.17 cells (Figure 1C), but interestingly both the Langat and influenza IIPs significantly decreased protein expression by 16-fold, with $p = 0.0097$ and 0.0061, respectively. In HeLa cells, many of the IIPs enhanced protein expression; HSV-2, HSV-1_1, HSV-1_2, Orf, and BVDV ranged from a 20- to 150-fold increase in *fLuc* expression. However, the PIV-5 V and MERS-CoV ORF4a proteins enhanced protein expression the most, with 796- and 893-fold, respectively, although only the PIV-5 group was statistically significant ($p = 0.0272$) while the ORF4a group was not ($p = 0.0689$). In MRC5 cells we similarly observed the greatest enhancement from the PIV-5 V and MERS-CoV ORF4a proteins, with 72- and 109-fold greater *fLuc* expression, with $p = 0.0485$ and 0.025, respectively. There was good agreement between expression levels from two independently prepared batches of RNA (Figure S1) in all cell types and for each construct.

We further investigated how two mutations to the PIV-5 V and MERS-CoV ORF4a protein affected protein expression in mouse (MEF), rabbit (RK13), nonhuman primate (LLC), and human (MRC5) cells (Figures S2A–S2D). The R172A mutation in PIV-5 V abrogates the ability to block MDA5 but not STAT,[41] and the K63A/K67A mutations in MERS-CoV ORF4a block binding to dsRNA.[42] We observed that the PIV-5 V and MERS-CoV ORF4a proteins did not enhance protein expression in MEF or RK13 cells. The MERS-CoV ORF4a protein did enhance protein expression in LLC and MRC5 cells (Figures S2C and S2D), and the K63A/K67A mutation greatly decreased the protein expression. The PIV-5 V protein enhanced protein expression in MRC5 cells but not in LLC cells, and the R172A mutation decreased protein expression in MRC5 cells. Overall these data indicate that the PIV-5 V and MERS-CoV ORF4a proteins enhanced protein expression in IFN-competent human cells, and mutating the proteins with the K63A/K67A and R172A substitutions known to reduce their anti-IFN activity muted saRNA expression.

MERS-CoV ORF4a Protein Partially Abates Increasing Dose Nonlinearity *In Vivo*

Given the enhancement of *in vitro* protein expression from the PIV-5 V and MERS-CoV ORF4a proteins, we then sought to determine whether these constructs could enhance protein expression *in vivo* and abate the nonlinearity of increasing the dose of saRNA. We tested saRNA encoding both *fLuc*, an intracellular protein, and *Gaussia* luciferase (*GLuc*), a secreted protein *in vivo* (Table 2). We chose to test these constructs in both BALB/c and C57BL/6 mice due to differences in the IFN-generating capacities: BALB/c mice are poor producers of IFN whereas C57BL/6 mice have been previously found to be the high producers of IFN-α/β and IFN-γ,[43] similar to the disparity of HEK293T.17 and HeLa/MRC5 cells *in vitro*. We observed that incorporating the PIV-5 V and MERS-CoV ORF4a proteins did not enhance protein expression of either *fLuc* or *GLuc* in BALB/c mice (Table 2; Figure S3). We observed slight enhancement of total area under the curve (AUC) protein expression of *fLuc* in C57BL/6 mice with the MERS-CoV ORF4a protein, and *GLuc* with both the PIV-5 V and MERS-CoV ORF4a proteins, although the differences were not statistically significant.

We have previously observed that increasing the dose of saRNA eventually results in a lower level of protein expression, and thus we sought to characterize whether the MERS-CoV ORF4a protein could abate the nonlinear dose dependency of saRNA *in vivo*. We tested doses of 0.2, 2, and 20 μg of the WT *fLuc* and the *fLuc* + MERS-CoV ORF4a replicon and quantified protein expression at days 7 and 10 after intramuscular (i.m.) injection (Figure 2). We observed that both constructs had similar protein expression (~5,000 photons/s) at a dose of 0.2 μg after 7 days, and protein expression increased for both (to ~50,000 photons/s for the WT and ~200,000 photons/s for the MERS-CoV ORF4a construct), when the dose was increased to 2 μg, although the incorporation of MERS-CoV ORF4a protein enhanced protein expression 4-fold, with $p = 0.0029$. Interestingly, both constructs exhibited lower protein expression at a dose of 20 μg after 7 days, although the WT was 18-fold lower than the MERS-CoV construct, with $p < 0.0001$. After 10 days the protein expression levels had equalized for the 2 μg dose, with no expression observed in the 0.2- and 20-μg doses. These data indicate that the MERS-CoV ORF4a protein enables partial rescue of the nonlinear dose dependence of saRNA *in vivo*.

Table 2. Area Under the Curve of Total Luciferase Expression in BALB/c and C57BL6/J during the Course of 14 days (n = 5)

	BALB/c			C57BL/6		
	WT	+ PIV-5	+ MERS-CoV ORF4a	WT	+ PIV-5	+ MERS-CoV ORF4a
fLuc	434,210 ± 173,923	235,231 ± 103,702	301,294 ± 170,309	263,783 ± 191,231	246,182 ± 87,859	453,411 ± 331,433
GLuc	1,950 ± 1,270	2,742 ± 493	1,596 ± 915	2,012 ± 1,373	4,513 ± 1,651	6,972 ± 2,789

Ruxolitinib Enhances Protein Expression of saRNA *In Vivo*

Given the role of the JAK/STAT pathway in the downstream IFN response, we then sought to characterize how combining saRNA, the MERS-CoV ORF4a IIP, and ruxolitinib, a potent, selective inhibitor of JAK1 and JAK2 protein kinases,[36] affects protein expression *in vivo* (Figure 3). We injected mice i.m. with 5 μg of saRNA encoding *fLuc* with and without MERS-CoV ORF4a with or without co-formulation with 100 μg of ruxolitinib and quantified protein expression 4, 7, 10, and 14 days after injection. After 4 days (Figure 3A), both of the formulations containing ruxolitinib had slightly higher protein expression (~10^6 photons/s) compared to the WT or MERS-CoV ORF4a constructs (~5×10^5 photons/s), although it was not statistically significant. However, after 7 days both of the formulations containing ruxolitinib had higher protein expression compared to the saRNA-only parallel groups, with $p = 0.0347$ and 0.0447, respectively. By day 10 these groups were still slightly elevated, but the difference was no longer statistically significant. After 14 days there was no protein expression observed in the saRNA groups without ruxolitinib, and only a few positive samples for the ruxolitinib groups. These data indicate that ruxolitinib enables a modest increase in saRNA protein expression but that there is no additive effect between the MERS-CoV ORF4a protein and ruxolitinib when combined.

PIV-5 V and MERS-CoV ORF4a Proteins Abate Increasing Dose Nonlinearity *Ex Vivo* in Human Skin Explants

As we observed that the IIPs exhibit differences in protein expression depending on the species of the cell type *in vitro*, we sought to test the saRNA IIP constructs in a more clinically relevant human skin explant model. We characterized both the quantity (% of enhanced green fluorescent protein [*EGFP*]$^+$ cells) and the quality of protein expression (median *EGFP* fluorescence intensity per cell) in resident human skin cells with incorporations of the PIV-5 V and MERS-CoV ORF4a proteins, as well as co-formulation with ruxolitinib (Figure 4). We tested doses of 0.2, 2, and 20 μg of the *EGFP* saRNA with the PIV-5 V and MERS-CoV ORF4a proteins (Figures 4A and 4B) and observed that increasing the dose of the WT construct from 0.2 to 2 μg resulted in an increase of the percentage of *EGFP*$^+$ cells from 10% to 18%, but when the dose was increased to 20 μg the percentage of *EGFP*$^+$ cells plummeted to ~5%. However, for the PIV-5 and MERS-CoV constructs, there was a linear dose increase with increasing dose of saRNA. The 0.2-μg dose similarly resulted in ~12% of *EGFP*$^+$ for both of these constructs, which further increased to 15% at 2 μg and 25% at 20 μg, at which point both the PIV-5 and MERS-CoV constructs had a statistically significantly higher percentage of *EGFP*$^+$ cells, with $p < 0.0001$ for both. Interestingly, neither the dose nor the incorporation of PIV-5 or MERS-CoV proteins affected the *EGFP* median fluorescence intensity (MFI), which was ~350 for all samples (Figure 4B). We further characterized which cells were expressing the saRNA using t-distributed stochastic neighbor embedding (tSNE), a type of principal component analysis for flow cytometry data that allows for visualization by unsupervised clustering of cells with overlaid defined protein and phenotype gating (Figures S4–S12).[44] We observed that at the highest dose of saRNA (20 μg), the PIV-5 V and MERS-CoV ORF4a proteins enabled protein expression in the immune cells, including T cells, dendritic cells, monocytes, B cells, Langerhans cells, leukocytes, and natural killer (NK) cells, as opposed to resident epithelial cells and fibroblasts.

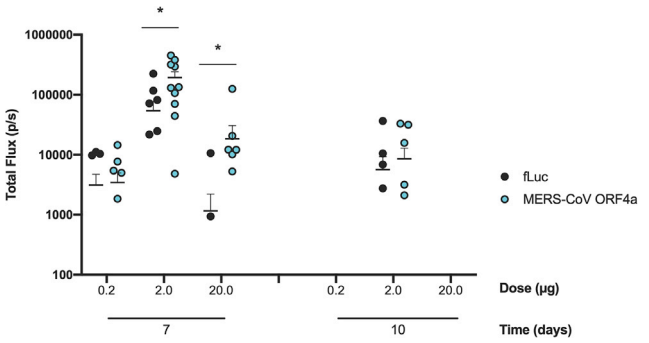

Figure 2. Dose Titration of WT and MERS-CoV ORF4a Replicon in C57BL6/J Mice

Protein expression was quantified at days 7 and 10 after intramuscular injection of either 0.2, 2, or 20 μg of RNA. Each dot represents a single mouse and the bar represents the mean ± SEM with n = 10. *$p < 0.05$ as evaluated using a Kruskal-Wallis test with multiple comparisons.

Next, we tested how incorporating doses of ruxolitinib, ranging from 0 to 100 μg, affected saRNA expression in human skin-resident cells. We observed that co-formulation of ruxolitinib with saRNA did not have any effect on the percentage of *EGFP*$^+$ cells (Figure 4C), although there was a slight trend that increasing the dose of ruxolitinib actually decreased the percentage of *EGFP*$^+$ cells from ~8% to ~5%. However, we did observe a profound effect on the per-cell quality of *EGFP* expression (Figure 4D); increasing the dose of ruxolitinib increased the *EGFP* MFI from ~100 to ~2,000 at a 10-μg dose of ruxolitinib, although the MFI decreased to ~1,000 with a 100-μg dose of ruxolitinib. Similarly, to the cells expressing the saRNA PIV-5 and MERS-CoV ORF4a proteins, we found that ruxolitinib enhanced protein expression in the immune cells, as opposed to epithelial cells and fibroblasts, and specifically increased uptake in T cells, Langerhans cells, leukocytes, and NK cells (Figures S13A and S13B).

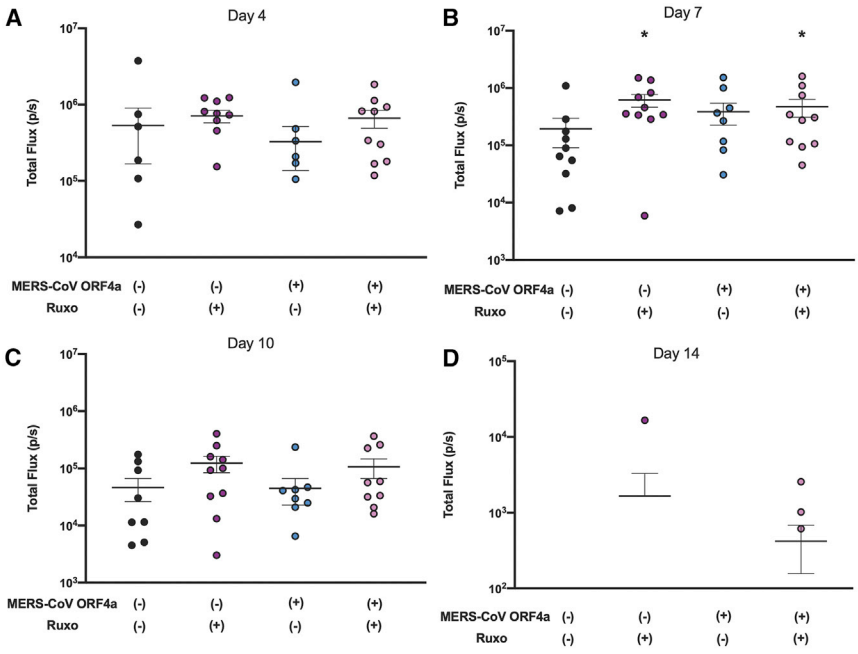

Figure 3. Co-formulation of WT and MERS-CoV ORF4a Replicons with JAK Inhibitor Ruxolitinib in C57BL6/J Mice

(A–D) Protein expression was quantified at days (A) 4, (B) 7, (C) 10, and (D) 14 after intramuscular injection of either 5 μg of RNA with 100 μg of ruxolitinib. Each dot represents a single mouse leg and the bar represents the mean ± SEM with n = 10. *p < 0.05 compared to WT *fLuc* using a Kruskal-Wallis test adjusted for multiple comparisons.

Taken together, these data show that the IIP replicons enhance expression in immune cells by increasing the percentage of cells expressing saRNA, while ruxolitinib enhances protein expression on a per cell basis.

MERS-CoV ORF4a Protein Enhances Immunogenicity of *RABV* Glycoprotein *In Vivo* in Rabbits

Because protein expression of nucleic acid formulations is not always a direct predictor of immunogenicity,[2] we then sought to characterize the immunogenicity of a model protein, the *RABV* glycoprotein, when combined with the MERS-CoV ORF4a protein. We injected rabbits with a primary dose of 20 μg of saRNA and a boost after 4 weeks, and then sampled the *RABV*-specific immunoglobulin G (IgG) antibodies in their blood at 0, 4, and 6 weeks (Figure 5A). We observed that all of the rabbits for both the WT and MERS-CoV ORF4a constructs seroconverted after a single injection. The IgG titers for the MERS-CoV group were slightly higher ($\sim 10^4$ ng/mL) compared to the WT ($\sim 5 \times 10^3$ ng/mL) after 4 weeks, but this was not statistically significant. However, after 6 weeks the antibody titers for animals in the MERS-CoV ORF4a group were significantly higher ($\sim 10^5$ ng/mL) compared to the WT ($\sim 10^4$ ng/mL), with p = 0.0061. The *RABV* pseudotyped neutralization reflected the antibody trends (Figure 5B). After 4 weeks the WT group had an average half-maximal inhibitory concentration (IC_{50}) of $\sim 10^3$, whereas the MERS-CoV group had an IC_{50} of $\sim 10^4$. After 6 weeks the MERS-CoV group had a much higher IC_{50} of $\sim 10^5$, whereas the WT group had stabilized at $\sim 10^3$. We also compared the immunogenicity of the WT *RABV* and *RABV*-MERS-CoV ORF4a saRNA in mice and rats (Figure S14) but did not observe any differences between the antibody titers or neutralization IC_{50} in either of these species. These data indicate that the MERS-CoV ORF4a protein enhances the immunogenicity of the *RABV* glycoprotein encoded by saRNA in rabbits, but not mice or rats.

MERS-CoV ORF4a and PIV-5 V Proteins Downregulate NF-κB and IRF3 Activation

In order to further probe the mechanism of action by which the IIPs enhance protein expression and immunogenicity of saRNA (Figure 6A), we transfected MRC5 cells with WT, MERS-CoV ORF4a, or PIV-5 V saRNA constructs and analyzed the quantities of active NF-κB and IRF3 in nuclear extracts after 4, 24, and 48 h (Figures 6B and 6C). We observed that active NF-κB was upregulated after 4 h in samples that were treated with WT *fLuc* saRNA or tumor necrosis factor (TNF)-α (positive control), which both had an optical density $(OD)_{450}$ of ~2.2, whereas the PIV-5 and ORF4a constructs significantly downregulated the quantity of active NF-κB to OD_{450} of 0.42 and 0.52 (p = 0.0049 and 0.0031), respectively. However, after 24 and 48 h the levels of active NF-κB decreased to OD_{450} <0.1 and <0.3 for the WT- and TNF-α-treated groups, and the PIV-5 and ORF4a groups returned to baseline. There was no active NF-κB in the untreated or pABOL control wells. The trends were similar but less pronounced for quantification of active IRF3. After 4 h there was an increase for the WT and TNF-α-treated groups, with an OD_{450} of 0.55 and 0.71, respectively. The PIV-5 and ORF4a groups were significantly lower, with OD_{450} levels of 0.34 and 0.35 (p = 0.0007 and 0.0011), respectively. After 24 h, the levels of active IRF3 were similar to 4 h, although the PIV-5 and ORF4a groups were equivalent at an OD_{450} of 0.25 and significantly lower than the WT and TNF-α-treated groups (p = 0.0029 and < 0.0001, respectively). After 48 h, the OD_{450} values for the WT, PIV-5, and ORF4a groups were not significantly different. The untreated and pABOL groups resulted in only a minimal increase in active IRF3 (OD_{450} of ~0.2) and did not vary over time. These data indicate that the PIV-5 V and MERS-CoV ORF4a proteins inhibit IFN activation in response to saRNA by downregulating NF-κB and IRF3 activity.

We also sought to determine whether saRNA stimulates cytokine production and whether these cytokines are affected by the ORF4a and PIV-5 V proteins, in both mouse and human peripheral blood mononuclear cells (PBMCs) (Figures S15 and S16). In mouse PBMCs, IFN-γ, interleukin (IL)-4, IL-5, IL-6, IL-23, TNF-α, IL-1β, MCP-1, MIP-1β, and MIP-2α were upregulated in response to saRNA, and

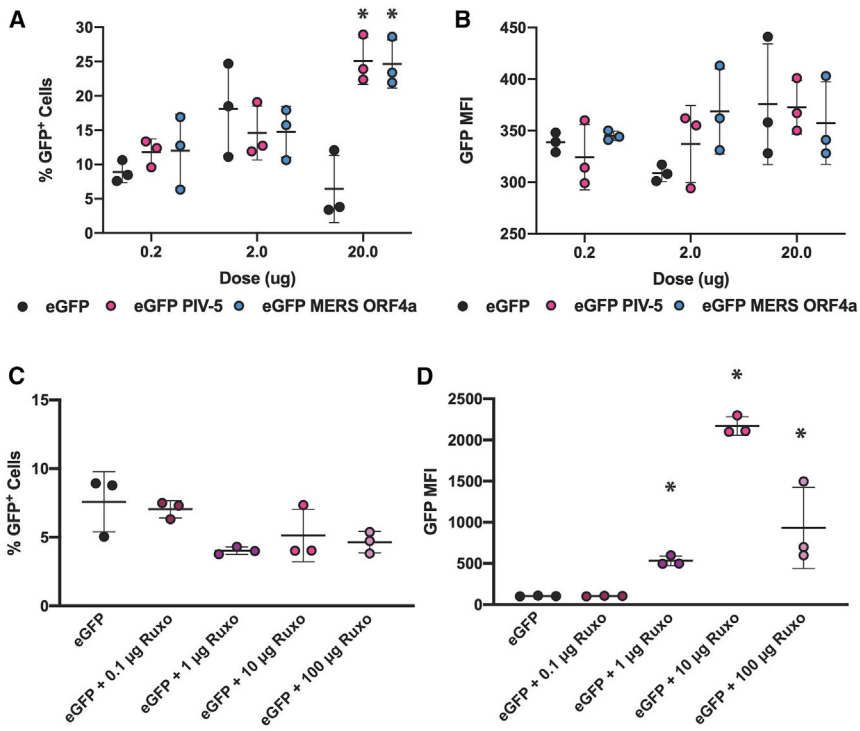

Figure 4. Protein Expression of *EGFP* in Human Skin Explants with or withouot IIPs and Ruxolitinib

(A–D) Protein expression of *EGFP* with and without MERS-CoV ORF4a RNA (0.2, 2, or 20 μg) (A and B) or with and without ruxolitinib (0.1, 1, 10, or 100 μg) (C and D) in human skin explants. Number of *EGFP* expression cells (%GFP$^+$ cells) (A and C) and total protein expression per cell (GFP median fluorescent intensity [MFI]) (B and D) were quantified 72 h after injection. Each dot represents a single explant and the bar represents the mean ± SEM with n = 3. *p < 0.05 as evaluated using a Kruskal-Wallis test with multiple comparisons.

there was slight but nonsignificant downregulation of IFN-γ, IL-4, and MIP-1α with the PIV-5 V and ORF4a constructs (Figure S15). For human PBMCs, IFN-α, IL-1β, IL-6, MIP-1β, and MIP-3α were upregulated in response to saRNA, and had similar slight but nonsignificant downregulation of IL-1α, IL-2, and MIP-3α with the IIP constructs (Figure S16). These data indicate that the sensing and regulation of innate activation differs between mouse and human cells and can be modulated using IIPs.

DISCUSSION

In this study, we screen a library of self-amplifying RNA with *cis*-encoded IIPs for protein expression *in vitro* in mouse, rabbit, nonhuman primate, and human cells, *ex vivo* in human skin explants, and *in vivo* in mice, as well as immunogenicity in mice, rats, and rabbits. We observed that the PIV-5 V and MERS-CoV ORF4a proteins enhanced protein expression 100- to 500-fold *in vitro* in IFN-competent HeLa and MRC5 cells. We found that the MERS-CoV ORF4a protein partially abates dose nonlinearity *in vivo*, and that ruxolitinib, but not the IIPs, enhances protein expression of saRNA *in vivo*. Both the PIV-5 V and MERS-CoV ORF4a proteins were found to enhance the percentage of resident cells in human skin explants expressing saRNA and completely rescued dose nonlinearity of saRNA, while ruxolitinib increased the protein expression on a per cell basis. We observed that the MERS-CoV ORF4a increased the *RABV*-specific IgG titer and neutralization IC_{50} by ∼10-fold in rabbits, but not mice or rats. Finally, we found that PIV-5 V and MERS-CoV ORF4a proteins downregulated IRF3 and NF-κB activation compared to WT saRNA.

After our *in vitro* screening, we chose to move forward with the MERS-CoV ORF4a replicon, as it was not feasible to screen all 10 candidates *in vivo*, and the PIV-5 V protein is not conserved between species (e.g., the N100D mutation needed for adaption to mice[45]) whereas the ORF4a protein is more highly conserved between species.[29–31] We observed that the R172A mutation to the PIV-5 V protein, which abrogates the ability to block binding to MDA5 but not STAT,[41] slightly inhibits protein expression in MRC5 cells (Figure S2D), thus indicating that binding to MDA5 is partially responsible for enhancing protein expression. Similarly, the K63A/K67A mutations of the MERS-CoV ORF4a protein limits the ability to bind dsRNA,[42,46] and they were observed to reduce protein expression in both nonhuman primate and human cells (Figures S2C and S2D). While a variety of the IIPs inhibit IFN by similar mechanisms to PIV-5 V and MERS-CoV ORF4a, the mechanism of action was not necessarily observed to be predictive of enhancing protein expression.

The protein designs, cells, and mutations characterized in these experiments offer insights into the mechanism by which the PIV-5 V and MERS-CoV ORF4a proteins increase protein expression (Figure 6). The PIV-5 V protein blocks MDA5 and IRF3 by binding to MDA5,[26,27] whereas the MERS-CoV ORF4a protein binds to dsRNA and suppresses protein activator of the IFN-induced protein kinase (PACT) triggering of MDA5 and RIG-I.[29–31] We observed that the PIV-5 V and ORF4a proteins downregulate IRF3 and NF-κB activation as compared to WT saRNA (Figures 6B and 6C). This is similar to previous studies, which show that MERS-CoV accessory proteins interfere with innate antiviral signaling pathways, including the NF-κB-mediated response.[47] While we observed minor differences in the mouse and human PBMC response to transfection with WT, PIV-5 V, and MERs-CoV ORF4a saRNA, this is likely due to low levels of transfection using pABOL (Figures S15 and S16). However, these results indicate that despite low levels of translation, the IIPs impact the cytokine profile of PBMCs and affect different cytokines depending on the species.

We have previously observed that protein expression of saRNA formulations is not necessarily predictive of immunogenicity,[2] and

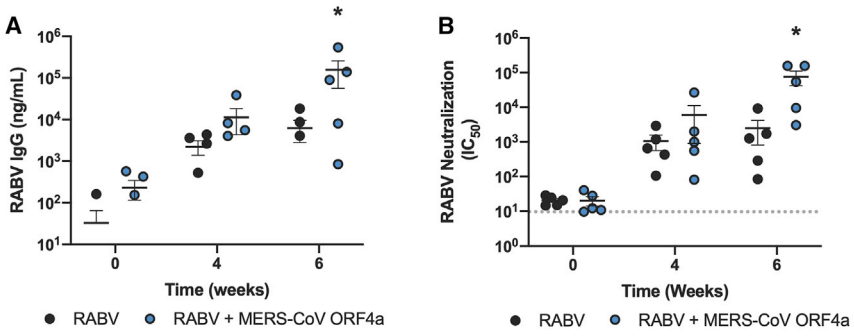

Figure 5. Immunogenicity of *RABV* with and without MERS-CoV ORF4a in Rabbits

(A) *RABV* antigen-specific IgG antibody titers following intramuscular immunization with prime and boost of 20 μg at 0 and 4 weeks, with n = 5. (B) Neutralization IC_{50} against pseudotyped *RABV* with n = 5; gray dotted line represents the limit of detection. Each dot represents one rabbit and the bar represents mean ± SEM with n = 5. *p < 0.05 as evaluated using a Kruskal-Wallis test with multiple comparisons.

thus we also characterized how the MERS-CoV ORF4a protein affected the immunogenicity of the rabies glycoprotein in mice, rats, and rabbits. We observed an increase in both the antibody titer and neutralization IC_{50} with the saRNA encoding *RABV* and MERS-CoV ORF4a (Figures 5A and 5B) in rabbits, but did not observe an increase in immunogenicity in mice or rats. While no preclinical animal model is perfectly predictive of human responses, rabbits are regarded as more immunologically similar to humans than mice or rats.[48–50] Furthermore, we did not observe any enhancement of protein expression by either the PIV-5 V or MERS-CoV ORF4a proteins in murine cells (Figure S2A), and thus the lack of enhancement of immunogenicity is not unexpected. We paired characterization in preclinical animal models with a human explant model, in which the cells are in a native tissue architecture and possess the inherent human IFN response. To our knowledge, we are the first to observe that the IIPs enhance the percentage of cells expressing saRNA, whereas ruxolitinib enhanced the expression per cell. We postulate that saRNA induces a binary state in a cell, wherein the replicase machinery enables maximal protein expression or the protein translation is massively inhibited by the IFN response. We have previously observed that the delivery system can be tailored to increase the percentage of cells expressing a reporter protein in a similar manner to the IIPs,[2,51–54] but the mechanism behind this is not well understood and warrants further studies. Given these promising results, we postulate that the MERS-CoV ORF4a protein may enhance immunogenicity of saRNA vaccines in humans, and it may also be useful for saRNA application to protein replacement therapies,[55,56] although clinical utility will require evaluation of any anti-vector immune response to the replicase or IIPs.

These experiments provide a proof of concept that IIPs can be directly encoded into saRNA vectors and effectively abate the nonlinear dose dependency and enhance immunogenicity. One limitation of this current study is that neither preclinical animal models nor human skin explants completely recapitulate the entire human immune system, which is the ultimate target of this work. As indicated by the mechanistic studies, different aspects of the IFN pathway can be targeted and increase saRNA expression, thus motivating probing of combinations of IIPs and other IFN inhibitions strategies, such as ruxolitinib. While these results are currently limited to preclinical animal models and human skin explants, future studies are warranted to study how these vectors enhance effectiveness of saRNA in human clinical trials.

MATERIALS AND METHODS

Self-Amplifying RNA Vectors

Self-amplifying RNA encoding *fLuc*, *GLuc*, *EGFP*, *RABV* glycoprotein, and the replicase derived from Venezuelan equine encephalitis were cloned into a plasmid vector, as previously described.[57] The library of IIPs was cloned into these vector backbones as part of the GOIs (*fLuc*, *GLuc*, *EGFP*, or *RABV*) with a T2A cleavage site (GenBank: AAC97195.1). The IIPs can be found with the following GenBank accession numbers: HSV-2 Us1 (GenBank: Z86099.2), HSV-1 Us1 (GenBank: AWO69381.1), HSV-1 Us11 (GenBank: YP_009137147.1), OV20.0L (GenBank: AF053969.1), BVDV Npro (GenBank: AIE38066.1), PIV-5 V (GenBank: YP_138513.1), MERS-CoV M (GenBank: AHC74104.1), MERS-CoV ORF4a (GenBank: AHC74090.1), Langat virus NS5 (GenBank: AF253420), and influenza virus NS1 (GenBank: DQ508893.1). For studies in mice, the PIV-5 V protein with an N100D mutation was used.[45]

In Vitro Transcription of saRNA

saRNA was produced using *in vitro* transcription. Plasmid DNA (pDNA) was transformed into *Escherichia coli* (New England Biolabs, UK) and cultured in 100 mL of Luria broth (LB) with 100 μg/mL of carbenicillin (Sigma-Aldrich, UK). The pDNA was subsequently isolated using a Plasmid Plus MaxiPrep kit (QIAGEN, UK), and the final concentration of pDNA was measured on a NanoDrop One (Thermo Fisher Scientific, UK). pDNA was linearized using MluI-HF for 3 h at 37°C. RNA for *in vitro* transfections was prepared using 1 μg of linearized pDNA template in a mMessage mMachine T7 transcription reaction (Invitrogen, UK) and purified using a MEGAclear transcription clean-up kit (Invitrogen, UK) using the manufacturer's protocol. RNA for *ex vivo* and *in vivo* experiments was prepared as previously described.[2] Uncapped RNA transcripts were produced using 1 μg of linearized pDNA template using a MEGAScript T7 transcription reaction (Invitrogen, UK) for 2 h at 37°C using the manufacturer's protocol. Transcripts were then purified by overnight LiCl precipitation at −20°C, centrifuged at 14,000 rpm for 20 min at 4°C to pellet the RNA, rinsed once with 70% EtOH, centrifuged again at 14,000 rpm for 5 min at 4°C. and resuspended in ultrapure H_2O (Ambion, UK). Purified transcripts were capped using the

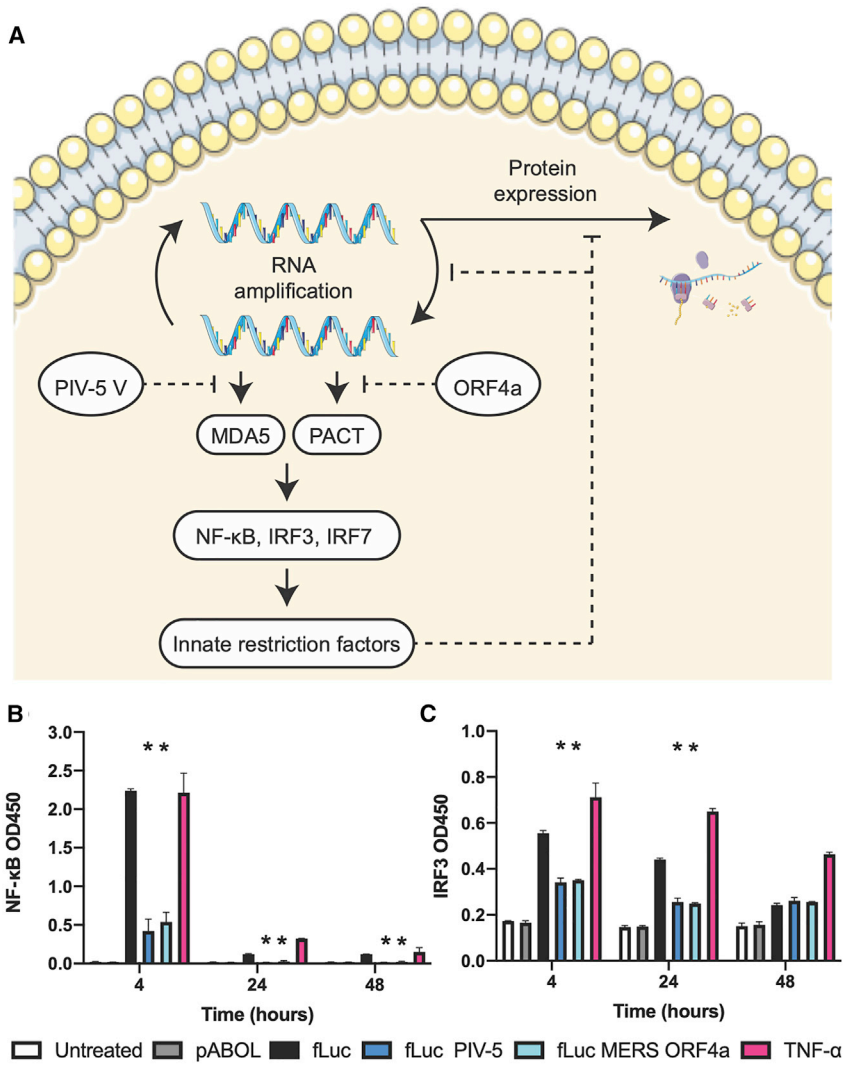

Figure 6. Mechanism of IIP Innate Inhibition of saRNA

(A) Schematic of proposed mechanism of PIV-5 V and MERS-CoV ORF4a on saRNA sensing. (B and C) Quantity of NF-κB (B) and IRF3 (C) in MRC5 cell nuclear extracts 4, 24, and 48 h after transfection, with n = 3. Bars represent mean ± standard deviation. *p < 0.05 compared to WT *fLuc* using a two-way ANOVA adjusted for multiple comparisons.

ScriptCap cap 1 capping system kit (Cellscript, WI, USA) for 2 h at 37°C using the manufacturer's protocol. Capped transcripts were then purified a final time with LiCl precipitation as described above, resuspended in RNA storage buffer (10 mM HEPES, 0.1 mM EDTA, and 100 mg/mL trehalose), and stored at −80°C until further use.

Preparation of RNA Polyplexes

fLuc, *GLuc*, and *EGFP* saRNA for protein expression experiments were complexed with 100-kDa pABOL using the titration method as previously described.[2] *RABV* saRNA for *in vivo* immunogenicity experiments was complexed with 8-kDa pABOL. Briefly, RNA and pABOL were diluted in HEPES buffer (20 mM HEPES, 5 wt % glucose in H_2O [pH 7.4]) and combined on a NanoAssemblr benchtop formulation unit (Precision Nanosystems, Vancouver, BC, Canada) at a volume ratio of 4:1 (RNA to polymer) with at flow rate of 10 mL/min. The final ratio of polymer to saRNA was 45:1 (w/w). Polyplexes were prepared fresh and used within 1 h of preparation. For co-formulations, ruxolitinib (ruxo, Selleck Chemicals, UK) was added directly to the polyplexes at the indicated doses.

In Vitro Transfection

Transfections were performed in HEK293T.17 cells (ATCC, USA), HeLa cells (ATCC, USA), MRC5 cells (ATCC, USA), mouse embryonic fibroblasts (MEFs) (Sigma-Aldrich, UK), RK13 rabbit kidney cells (Public Health England, UK), and LLC-MK2 rhesus macaque kidney cells (ATCC, USA). Cells were cultured in complete Dulbecco's modified Eagle's medium (cDMEM) (Gibco, Thermo Fisher Scientific, UK) containing 10% (v/v) fetal bovine serum (FBS), 5 mg/mL L-glutamine, and 5 mg/mL penicillin/streptomycin (Thermo Fisher Scientific, UK) (HEK cells, HeLa cells, MEFs), complete modified Eagle's medium (cMEM) with 10% (v/v) FBS, 5 mg/mL L-glutamine, and 5 mg/mL penicillin/streptomycin (Thermo Fisher Scientific, UK) (MRC5, RK13 cells), or complete medium 199 (cM199, Sigma-Aldrich, UK) with 1% horse serum (Gibco, Thermo Fisher Scientific, UK) (LLC cells). Cells were plated at a density of 50,000 cells per well in a clear 96-well plate 24 h prior to transfection. Culture medium was then completely removed and replaced with 50 μL of pre-warmed transfection medium (DMEM + 5 mg/mL L-glutamine, MEM + 5 mg/mL L-glutamine or M199). Then, 100 μL of the polyplex solution (containing 100 ng of saRNA) was added to each well and allowed to incubate for 4 h. Transfection medium was then completely removed and replaced with cDMEM, cMEM, or cM199. After 24 h, 50 μL of medium was removed from each well and 50 μL of ONE-Glo D-luciferin substrate (Promega, UK) was added and mixed well by pipetting. The total volume from each well was then transferred to a white 96-well plate (Costar) for analysis and quantified on a FLUOstar Omega plate reader (BMG Labtech, UK). Background fluorescence from the control wells was subtracted from each well.

In Vivo Luciferase Expression in Mice

All animals were handled in accordance with the UK Home Office Animals Scientific Procedures Act 1986 and with a local ethics board and UK government-approved project license (P63FE629C) and personal license (IC37CBB8F). Food and water were supplied *ad libitum*.

Female BABL/c mice (Charles River, UK) or C57BL/6 mice (Charles River, UK), aged 6–8 weeks, were housed in groups (n = 5 per cage) and housed in a fully acclimatized room. Mice were injected i.m. with either 5 μg of *fLuc* saRNA in both hind legs or 5 μg of *GLuc* in one hind leg, complexed with pABOL in a total volume of 50 μL. After 3, 4, 7, 10, or 14 days the mice were imaged for *fLuc* as previously described[58,59] or blood was collected for *GLuc* analysis using a Gaussia Luciferase Glow Assay kit (Pierce, Thermo Scientific, UK) according to the manufacturer's protocol. The protein expression in the sera was quantified on a FLUOstar Omega plate reader (BMG Labtech, UK). Background fluorescence from the control wells was subtracted from each well. For *fLuc* analysis, the mice were injected intraperitoneally (i.p.) with 150 μL of XenoLight RediJect D-luciferin substrate (PerkinElmer, UK) and allowed to rest for 10 min. Mice were then anesthetized using isoflurane and imaged on an *in vivo* imaging system (IVIS) FX Pro (Kodak, Rochester, NY, USA) equipped with Molecular Imaging software version 5.0 (Carestream Health, USA) for 2 min. Signal from each injection site was quantified using Molecular Imaging software and expressed as total flux (photons/s).

Vaccination of Mice, Rats, and Rabbits

BALB/c mice, Sprague-Dawley rats, and New Zealand White rabbits were immunized with 1 μg (mice) or 20 μg (rats, rabbits) of *RABV*-encoding saRNA formulated with pABOL in a total volume of 50 μL (mice) or 100 μL (rats, rabbits) i.m. in one hind leg. A boost injection was given 4 weeks after the initial prime. Blood was collected after 0, 4, and 6 weeks from study onset and centrifuged at 10,000 rpm for 5 min. Sera were then decanted and stored at −80°C until further analysis.

RABV-Specific ELISAs

A semiquantitative Ig ELISA protocol was performed as previously described.[60] Briefly, 0.5 μg/mL of *RABV*-coated ELISA plates was blocked with 1% (w/v) bovine serum albumin (BSA) and 0.05% (v/v) Tween 20 in PBS. After washing, diluted serum samples were added to the plates and incubated for 1 h. The plates were then washed and a 1:4,000 dilution of anti-mouse IgG-horseradish peroxidase (HRP) (SouthernBiotech, UK) was added for the mouse ELISAs, a 1:4,000 dilution of goat anti-rat IgG-HRP (SouthernBiotech, UK) was added for the rat ELISAs, and a 1:10,000 dilution of mouse anti-rabbit IgG-HRP (Sigma, UK) was added for the rabbit ELISAs. Mouse standards were prepared by coating ELISA plate wells with anti-mouse kappa (1:1,000) and lambda (1:1,000) light chains (AbD Serotec, UK), blocking with 1% (w/v) BSA/0.05% (v/v) Tween 20 in PBS, washing, and adding purified IgG (SouthernBiotech, UK) starting at 1,000 ng/mL and titrating down with a 5-fold dilution series. Rat standards were prepared by directly coating ELISA plate wells with purified rat IgG (R&D Systems, UK) starting at 1,000 ng/mL and titrating down with a 5-fold dilution series. Rabbit standards were prepared by coating ELISA plate wells with a 1:1,250 dilution of goat anti-rabbit IgG Fc (Millipore, UK), blocking with 1% (w/v) BSA/0.05% (v/v) Tween 20 in PBS, washing, and adding purified rabbit IgG (AbD Serotec, UK) starting at 1,000 ng/mL and titrating down with a 5-fold dilution series. Samples and standard were developed using 3,3′,5,5′-tetramethylbenzidine (TMB). The reaction was stopped after 5 min with stop solution (Insight Biotechnologies, UK). Absorbance was read on a spectrophotometer (VersaMax, Molecular Devices, UK) with SoftMax Pro GxP v5 software.

RABV Microneutralization Assay

Pseudotyped rabies microneutralization was performed on week 0, 4, and 6 samples. BHK-21 cells were seeded at 10,000 cells/well in cDMEM in a 96-well plate. Sera were heat-inactivated at 56°C and then diluted in a 1:5 serial dilution in cDMEM. Samples were then diluted with an equal volume of pseudo-virus at a concentration of 100 $TCID_{50}$ (50% tissue culture infective dose) in 50 μL, incubated for 1 h at 37°C, and then added to BHK-21 cells and cultured for 48 h at 37°C. Cells were then lysed and luciferase activity was quantified using a Bright-Glo luciferase assay (Promega, UK). The total volume from each well was then transferred to a white 96-well plate (Costar) for analysis and quantified on a FLUOstar Omega plate reader (BMG Labtech, UK) and the IC_{50} was calculated for each sample.

Human Skin Explant Culture and Injection

For *ex vivo* studies, surgically resected specimens of human skin tissues were collected at Charing Cross Hospital, Imperial NHS Trust, London, UK. All tissues were collected after receiving signed informed consent from patients undergoing elective abdominoplasty or mastectomy surgeries, under protocols approved by the Local Research Ethics Committee (MED_RS_11_014) at Imperial College London. Skin tissue was refrigerated until use and was excised into 1-cm^2 section and cultured in 12-well plates with 2 mL of cDMEM at 37°C with 5% CO_2. Explants were injected intradermally (i.d.) using a BD Micro-Fine Demi 0.3-mL syringe (Becton Dickinson, UK) with a dose of 2 μg of saRNA in a total volume of 50 μL. Media were replaced daily for the duration of culture.

Flow Cytometry

After 72 h from the time of injection, skin explants were trimmed to remove the subcutaneous fat layer, and the epidermal and dermal layers were minced well with scissors and incubated in 2 mL of DMEM supplemented with 1 mg/mL collagenase P (Sigma-Aldrich, UK) and 5 mg/mL Dispase II (Sigma-Aldrich, UK) for 4 h at 37°C on a rotational shaker. Digests were then filtered through a 70-μm cell strainer and centrifuged at 1,750 rpm for 5 min. Cells were then resuspended in 100 μL of fluorescence-activated cell sorting (FACS) buffer (PBS + 2.5% FBS) and stained with fixable aqua Live/Dead cell stain (Thermo Fisher Scientific, UK) diluted 1:400 in FACS buffer for 20 min on ice. Samples were then washed with 1 mL of FACS buffer, centrifuged at 1,750 rpm for 5 min, and stained with a mixture of the following antibodies: CD3-V450 (BioLegend, UK), CD14-Qdot605 (BioLegend, UK), CD19-Brilliant Violet (BV) 650 (BioLegend, UK), CD56-BV711 (BioLegend, UK), CD1a-peridinin chlorophyll protein (PerCP)-eFluor 710 (BioLegend, UK), CD11c-phycoerythrin (PE) (BioLegend, UK), CD90-PE-Cy7 (BioLegend, UK), and CD45-Alexa Fluor (AF)700 (BioLegend, UK). Samples were them washed with 1 mL of FACS buffer, centrifuged at

1,750 rpm for 5 min, resuspended in 250 μL of PBS, and then fixed with 250 μL of 3% paraformaldehyde for a final concentration of 1.5% paraformaldehyde, and refrigerated until flow cytometry analysis. Samples were analyzed on an LSRFortessa (BD Biosciences, UK) flow cytometer with FACSDiva software (BD Biosciences, UK) with 100,000 acquired cell events. Gating strategy was performed as previously described,[54] and phenotypic identity of GFP^+ cells was quantified using FlowJo version 10 (FlowJo, OR, USA). t-Distributed stochastic neighbor embedding analysis of unsupervised clusters of live cells was performed in FlowJo using 1,000 iterations, a perplexity of 30, a learning rate of 15,196, the Exact (vantage point tree) k-nearest neighbors (KNN) algorithm, and the Barnes-Hut gradient algorithm.

Transcription Factor ELISAs

MRC5 cells were cultured in cDMEM and plated at a density of 1.5×10^6 cells per well in a clear six-well plate 24 h prior to transfection. Culture medium was then completely removed and replaced with 250 μL of pre-warmed transfection medium and 250 μL of the polyplex solution (containing 3 μg of saRNA) was added to each well and allowed to incubate for 4 h. Transfection medium was then completely removed and replaced with cDMEM. Positive control wells were stimulated with 20 mM TNF-α in cDMEM. After 4, 24, or 48 h the nuclear extract was harvested using a nuclear extract kit (Active Motif, Belgium) according to the manufacturer's protocol. The nuclear extracts were analyzed using an IRF3 and NF-κB ELISA kit (Active Motif, Belgium) according to the manufacturer's protocol and the optical density at a wavelength of 450 nm (OD_{450}) was quantified on a FLUOstar Omega plate reader (BMG Labtech, UK).

Cytokine Measurement in PBMCs

PBMCs were harvested from mouse and human blood and plated at a density of 125,000 cells per well in a clear 96-well plate and immediately transfected. 50 μL of pre-warmed transfection medium and 50 μL of the polyplex solution (containing 100 ng of saRNA) were added to each well for 4 h. Transfection media were then removed, and the cells were cultured with cDMEM supplemented with 0.1 mM β-mercaptoethanol (Sigma-Aldrich, UK) for 4, 24, and 48 h. Positive control wells were stimulated with 20 mM TNF-α in cDMEM. At each time point, 50 μL of the culture media was removed and frozen at −80°C until further cytokine analysis. Then, 50 μL of ONE-Glo D-luciferin substrate (Promega, UK) was added and mixed well by pipetting. The total volume from each well was then transferred to a white 96-well plate (Costar) for analysis and quantified on a FLUOstar Omega plate reader (BMG Labtech, UK). The cytokine response in each well was quantified with a custom mouse or human 25-plex ProcartaPlex immunoassay (Thermo Fisher Scientific, UK) on a Bio-Plex 200 system (Bio-Rad) according to the manufacturer's instructions.

Statistical Analysis

Graphs and statistics were prepared in GraphPad Prism, version 8. Statistical differences were analyzed using either a two-way ANOVA or a Kruskal-Wallis test adjusted for multiple comparisons, with $p < 0.05$ used to indicate significance.

SUPPLEMENTAL INFORMATION

Supplemental Information can be found online at https://doi.org/10.1016/j.ymthe.2020.11.011.

ACKNOWLEDGMENTS

We gratefully acknowledge the surgeons at Charing Cross Hospital, E. Dex and J. Hunter, and their nursing team for providing the tissue used in these experiments, and Jonathan Yeow for providing the pA-BOL polymer for these studies. A.K.B. was supported by a Whitaker Post-Doctoral Fellowship and a Marie Skłodowska Curie Individual Fellowship funded by the European Commission H2020 (no. 794059). P.F.M., C.R.B., K.H., K.S., and R.J.S. were funded by the Department of Health & Social Care using UK Aid funding and is managed by the Engineering and Physical Sciences Research Council (EPSRC, grant no. EP/R013764/1; note that the views expressed in this publication are those of the authors and not necessarily those of the Department of Health and Social Care). We also acknowledge Dormeur Investment Services for providing funds to purchase equipment used in these studies.

AUTHOR CONTRIBUTIONS

A.K.B., P.F.M., and R.J.S. conceptualized the vector and study design. A.K.B. and C.R.B. performed the *in vitro* experiments. A.K.B., P.F.M., K.H., and K.S. performed the *in vivo* studies, aided by C.R.B. A.K.B. analyzed the data and wrote the manuscript with constructive feedback from P.F.M., C.R.B., K.H., K.S., and R.J.S.

DECLARATION OF INTERESTS

A.K.B., P.F.M., and R.J.S. are co-inventors of a patent resulting from this work. The remaining authors declare no competing interests.

REFERENCES

1. Perri, S., Greer, C.E., Thudium, K., Doe, B., Legg, H., Liu, H., Romero, R.E., Tang, Z., Bin, Q., Dubensky, T.W., Jr., et al. (2003). An alphavirus replicon particle chimera derived from Venezuelan equine encephalitis and Sindbis viruses is a potent gene-based vaccine delivery vector. J. Virol. *77*, 10394–10403.

2. Blakney, A.K., Zhu, Y., McKay, P.F., Bouton, C.R., Yeow, J., Tang, J., Hu, K., Samnuan, K., Grigsby, C.L., Shattock, R.J., and Stevens, M.M. (2020). Big is beautiful: enhanced saRNA delivery and immunogenicity by a higher molecular weight, bioreducible, cationic polymer. ACS Nano *14*, 5711–5727.

3. Brito, L.A., Chan, M., Shaw, C.A., Hekele, A., Carsillo, T., Schaefer, M., Archer, J., Seubert, A., Otten, G.R., Beard, C.W., et al. (2014). A cationic nanoemulsion for the delivery of next-generation RNA vaccines. Mol. Ther *22*, 2118–2129.

4. Blakney, A.K., McKay, P.F., Yus, B.I., Aldon, Y., and Shattock, R.J. (2019). Inside out: optimization of lipid nanoparticle formulations for exterior complexation and in vivo delivery of saRNA. Gene Ther. *26*, 363–372.

5. Geall, A.J., Verma, A., Otten, G.R., Shaw, C.A., Hekele, A., Banerjee, K., Cu, Y., Beard, C.W., Brito, L.A., Krucker, T., et al. (2012). Nonviral delivery of self-amplifying RNA vaccines. Proc. Natl. Acad. Sci. USA *109*, 14604–14609.

6. Chahal, J.S., Khan, O.F., Cooper, C.L., McPartlan, J.S., Tsosie, J.K., Tilley, L.D., Sidik, S.M., Lourido, S., Langer, R., Bavari, S., et al. (2016). Dendrimer-RNA nanoparticles generate protective immunity against lethal Ebola, H1N1 influenza, and *Toxoplasma gondii* challenges with a single dose. Proc. Natl. Acad. Sci. USA *113*, E4133–E4142.

7. Vogel, A.B., Lambert, L., Kinnear, E., Busse, D., Erbar, S., Reuter, K.C., Wicke, L., Perkovic, M., Beissert, T., Haas, H., et al. (2018). Self-amplifying RNA vaccines give equivalent protection against influenza to mRNA vaccines but at much lower doses. Mol. Ther. *26*, 446–455.

8. Kallen, K.J., Heidenreich, R., Schnee, M., Petsch, B., Schlake, T., Thess, A., Baumhof, P., Scheel, B., Koch, S.D., and Fotin-Mleczek, M. (2013). A novel, disruptive vaccination technology: self-adjuvanted RNActive® vaccines. Hum. Vaccin. Immunother. *9*, 2263–2276.

9. Pardi, N., Hogan, M.J., Porter, F.W., and Weissman, D. (2018). mRNA vaccines—a new era in vaccinology. Nat. Rev. Drug Discov. *17*, 261–279.

10. de Haro, C., Méndez, R., and Santoyo, J. (1996). The eIF-2α kinases and the control of protein synthesis. FASEB J. *10*, 1378–1387.

11. Liang, S.L., Quirk, D., and Zhou, A. (2006). RNase L: its biological roles and regulation. IUBMB Life *58*, 508–514.

12. Alberer, M., Gnad-Vogt, U., Hong, H.S., Mehr, K.T., Backert, L., Finak, G., Gottardo, R., Bica, M.A., Garofano, A., Koch, S.D., et al. (2017). Safety and immunogenicity of a mRNA rabies vaccine in healthy adults: an open-label, non-randomised, prospective, first-in-human phase 1 clinical trial. Lancet *390*, 1511–1520.

13. Hagai, T., Chen, X., Miragaia, R.J., Rostom, R., Gomes, T., Kunowska, N., Henriksson, J., Park, J.E., Proserpio, V., Donati, G., et al. (2018). Gene expression variability across cells and species shapes innate immunity. Nature *563*, 197–202.

14. Kim, D.Y., Atasheva, S., McAuley, A.J., Plante, J.A., Frolova, E.I., Beasley, D.W.C., and Frolov, I. (2014). Enhancement of protein expression by alphavirus replicons by designing self-replicating subgenomic RNAs. Proc. Natl. Acad. Sci. USA *111*, 10708–10713.

15. Pepini, T., Pulichino, A.M., Carsillo, T., Carlson, A.L., Sari-Sarraf, F., Ramsauer, K., Debasitis, J.C., Maruggi, G., Otten, G.R., Geall, A.J., et al. (2017). Induction of an IFN-mediated antiviral response by a self-amplifying RNA vaccine: implications for vaccine design. J. Immunol. *198*, 4012–4024.

16. Devasthanam, A.S. (2014). Mechanisms underlying the inhibition of interferon signaling by viruses. Virulence *5*, 270–277.

17. Liu, Y., Chin, J.M., Choo, E.L., and Phua, K.K.L. (2019). Messenger RNA translation enhancement by immune evasion proteins: a comparative study between EKB (vaccinia virus) and NS1 (influenza A virus). Sci. Rep. *9*, 11972.

18. Beissert, T., Koste, L., Perkovic, M., Walzer, K.C., Erbar, S., Selmi, A., Diken, M., Kreiter, S., Türeci, Ö., and Sahin, U. (2017). Improvement of in vivo expression of genes delivered by self-amplifying RNA using vaccinia virus immune evasion proteins. Hum. Gene Ther. *28*, 1138–1146.

19. Zhang, M., Liu, Y., Wang, P., Guan, X., He, S., Luo, S., Li, C., Hu, K., Jin, W., Du, T., et al. (2015). HSV-2 immediate-early protein US1 inhibits IFN-β production by suppressing association of IRF-3 with IFN-β promoter. J. Immunol. *194*, 3102–3115.

20. Kew, C., Lui, P.-Y., Chan, C.-P., Liu, X., Au, S.W.N., Mohr, I., Jin, D.Y., and Kok, K.H. (2013). Suppression of PACT-induced type I interferon production by herpes simplex virus 1 Us11 protein. J. Virol. *87*, 13141–13149.

21. Xing, J., Wang, S., Lin, R., Mossman, K.L., and Zheng, C. (2012). Herpes simplex virus 1 tegument protein US11 downmodulates the RLR signaling pathway via direct interaction with RIG-I and MDA-5. J. Virol. *86*, 3528–3540.

22. Tseng, Y.Y., Liao, G.R., Sen, G.C., Lin, F.Y., and Hsu, W.L. (2015). Regulation of PACT-mediated protein kinase activation by the OV20.0 protein of Orf virus. J. Virol. *89*, 11619–11629.

23. Haig, D.M., McInnes, C.J., Thomson, J., Wood, A., Bunyan, K., and Mercer, A. (1998). The orf virus OV20.0L gene product is involved in interferon resistance and inhibits an interferon-inducible, double-stranded RNA-dependent kinase. Immunology *93*, 335–340.

24. Horscroft, N., Bellows, D., Ansari, I., Lai, V.C., Dempsey, S., Liang, D., Donis, R., Zhong, W., and Hong, Z. (2005). Establishment of a subgenomic replicon for bovine viral diarrhea virus in Huh-7 cells and modulation of interferon-regulated factor 3-mediated antiviral response. J. Virol. *79*, 2788–2796.

25. Darweesh, M.F., Rajput, M.K.S., Braun, L.J., Rohila, J.S., and Chase, C.C.L. (2018). BVDV Npro protein mediates the BVDV induced immunosuppression through interaction with cellular S100A9 protein. Microb. Pathog. *121*, 341–349.

26. Rodriguez, K.R., and Horvath, C.M. (2014). Paramyxovirus V protein interaction with the antiviral sensor LGP2 disrupts MDA5 signaling enhancement but is not relevant to LGP2-mediated RLR signaling inhibition. J. Virol. *88*, 8180–8188.

27. Mandhana, R., Qian, L.K., and Horvath, C.M. (2018). Constitutively active MDA5 proteins are inhibited by paramyxovirus V proteins. J. Interferon Cytokine Res. *38*, 319–332.

28. Lui, P.Y., Wong, L.Y., Fung, C.L., Siu, K.L., Yeung, M.L., Yuen, K.S., Chan, C.P., Woo, P.C., Yuen, K.Y., and Jin, D.Y. (2016). Middle East respiratory syndrome coronavirus M protein suppresses type I interferon expression through the inhibition of TBK1-dependent phosphorylation of IRF3. Emerg. Microbes Infect. *5*, e39.

29. Yang, Y., Zhang, L., Geng, H., Deng, Y., Huang, B., Guo, Y., Zhao, Z., and Tan, W. (2013). The structural and accessory proteins M, ORF 4a, ORF 4b, and ORF 5 of Middle East respiratory syndrome coronavirus (MERS-CoV) are potent interferon antagonists. Protein Cell *4*, 951–961.

30. Shokri, S., Mahmoudvand, S., Taherkhani, R., and Farshadpour, F. (2019). Modulation of the immune response by Middle East respiratory syndrome coronavirus. J. Cell. Physiol. *234*, 2143–2151.

31. Batool, M., Shah, M., Patra, M.C., Yesudhas, D., and Choi, S. (2017). Structural insights into the Middle East respiratory syndrome coronavirus 4a protein and its dsRNA binding mechanism. Sci. Rep. *7*, 11362.

32. Comar, C.E., Goldstein, S.A., Li, Y., Yount, B., Baric, R.S., and Weiss, S.R. (2019). Antagonism of dsRNA-induced innate immune pathways by NS4a and NS4b accessory proteins during MERS coronavirus infection. MBio *10*, e00319-19.

33. Best, S.M. (2017). The many faces of the flavivirus NS5 protein in antagonism of type i interferon signaling. J. Virol. *91*, e01970-16.

34. Werme, K., Wigerius, M., and Johansson, M. (2008). Tick-borne encephalitis virus NS5 associates with membrane protein scribble and impairs interferon-stimulated JAK-STAT signalling. Cell. Microbiol. *10*, 696–712.

35. Krug, R.M. (2015). Functions of the influenza A virus NS1 protein in antiviral defense. Curr. Opin. Virol. *12*, 1–6.

36. Elli, E.M., Baratè, C., Mendicino, F., Palandri, F., and Palumbo, G.A. (2019). Mechanisms underlying the anti-inflammatory and immunosuppressive activity of ruxolitinib. Front. Oncol. *9*, 1186.

37. Fitzgerald, M.E., Rawling, D.C., Potapova, O., Ren, X., Kohlway, A., and Pyle, A.M. (2017). Selective RNA targeting and regulated signaling by RIG-I is controlled by coordination of RNA and ATP binding. Nucleic Acids Res. *45*, 1442–1454.

38. Hemmi, H., Takeuchi, O., Sato, S., Yamamoto, M., Kaisho, T., Sanjo, H., Kawai, T., Hoshino, K., Takeda, K., and Akira, S. (2004). The roles of two IκB kinase-related kinases in lipopolysaccharide and double stranded RNA signaling and viral infection. J. Exp. Med. *199*, 1641–1650.

39. Cantell, K. (1961). Production and action of interferon in HeLa cells. Arch. Gesamte Virusforsch. *10*, 510–521.

40. Meurs, E., Hovanessian, A.G., and Montagnier, L. (1981). Interferon-mediated antiviral state in human MRC5 cells in the absence of detectable levels of 2-5A synthetase and protein kinase. J. Interferon Res. *1*, 219–232.

41. Ramachandran, A., and Horvath, C.M. (2010). Dissociation of paramyxovirus interferon evasion activities: universal and virus-specific requirements for conserved V protein amino acids in MDA5 interference. J. Virol. *84*, 11152–11163.

42. Siu, K.-L., Yeung, M.L., Kok, K.-H., Yuen, K.-S., Kew, C., Lui, P.-Y., Chan, C.P., Tse, H., Woo, P.C., Yuen, K.Y., and Jin, D.Y. (2014). Middle East respiratory syndrome coronavirus 4a protein is a double-stranded RNA-binding protein that suppresses PACT-induced activation of RIG-I and MDA5 in the innate antiviral response. J. Virol. *88*, 4866–4876.

43. Shirahata, T., Mori, A., Ishikawa, H., and Goto, H. (1986). Strain differences of interferon-generating capacity and resistance in toxoplasma-infected mice. Microbiol. Immunol. *30*, 1307–1316.

44. Van Der Maaton, L., and Hinton, G. (2008). Visualizing data using t-SNE. J. Mach. Learn. Res. *9*, 2579–2605.

45. Kraus, T.A., Garza, L., and Horvath, C.M. (2008). Enabled interferon signaling evasion in an immune-competent transgenic mouse model of parainfluenza virus 5 infection. Virology *371*, 196–205.

46. Rabouw, H.H., Langereis, M.A., Knaap, R.C.M., Dalebout, T.J., Canton, J., Sola, I., Enjuanes, L., Bredenbeek, P.J., Kikkert, M., de Groot, R.J., and van Kuppeveld, F.J. (2016). Middle East respiratory coronavirus accessory protein 4a inhibits PKR-mediated antiviral stress responses. PLoS Pathog. *12*, e1005982.

47. Canton, J., Fehr, A.R., Fernandez-Delgado, R., Gutierrez-Alvarez, F.J., Sanchez-Aparicio, M.T., García-Sastre, A., Perlman, S., Enjuanes, L., and Sola, I. (2018). MERS-CoV 4b protein interferes with the NF-κB-dependent innate immune response during infection. PLoS Pathog. *14*, e1006838.

48. Jameson, S.C., and Masopust, D. (2018). What is the predictive value of animal models for vaccine efficacy in humans? Reevaluating the potential of mouse models for the human immune system. Cold Spring Harb. Perspect. Biol. *10*, a029132.

49. Gerdts, V., Wilson, H.L., Meurens, F., van Drunen Littel-van den Hurk, S., Wilson, D., Walker, S., Wheler, C., Townsend, H., and Potter, A.A. (2015). Large animal models for vaccine development and testing. ILAR J. *56*, 53–62.

50. Vaure, C., and Liu, Y. (2014). A comparative review of toll-like receptor 4 expression and functionality in different animal species. Front. Immunol. *5*, 316.

51. Saviano, F., Lovato, T., Russo, A., Russo, G., Bouton, C.R., Shattock, R.J., Alexander, C., Quaglia, F., Blakney, A.K., Gurnani, P., and Conte, C. (2020). Ornithine-derived oligomers and dendrimers for in vitro delivery of DNA and ex vivo transfection of skin cells via saRNA. J. Mater. Chem. B Mater. Biol. Med. *8*, 4940–4949.

52. Blakney, A.K., Abdouni, Y., Yilmaz, G., Liu, R., McKay, P.F., Bouton, C.R., Shattock, R.J., and Becer, C.R. (2020). Mannosylated poly(ethylene imine) copolymers enhance saRNA uptake and expression in human skin explants. Biomacromolecules *21*, 2482–2492.

53. Gurnani, P., Blakney, A.K., Terracciano, R., Petch, J.E., Blok, A.J., Bouton, C.R., McKay, P.F., Shattock, R.J., and Alexander, C. (2020). The *in vitro*, *ex vivo*, and *in vivo* effect of polymer hydrophobicity on charge-reversible vectors for self-amplifying RNA. Biomacromolecules *21*, 3242–3253.

54. Blakney, A.K., McKay, P.F., Ibarzo Yus, B., Hunter, J.E., Dex, E.A., and Shattock, R.J. (2019). The skin you are in: design-of-experiments optimization of lipid nanoparticle self-amplifying RNA formulations in human skin explants. ACS Nano *13*, 5920–5930.

55. Magadum, A., Kaur, K., and Zangi, L. (2019). mRNA-based protein replacement therapy for the heart. Mol. Ther. *27*, 785–793.

56. Kowalski, P.S., Rudra, A., Miao, L., and Anderson, D.G. (2019). Delivering the messenger: advances in technologies for therapeutic mRNA delivery. Mol. Ther *27*, 710–728.

57. Blakney, A.K., McKay, P.F., and Shattock, R.J. (2018). Structural components for amplification of positive and negative strand VEEV splitzicons. Front. Mol. Biosci. *5*, 71.

58. Blakney, A.K., McKay, P.F., Christensen, D., Yus, B.I., Aldon, Y., Follmann, F., and Shattock, R.J. (2019). Effects of cationic adjuvant formulation particle type, fluidity and immunomodulators on delivery and immunogenicity of saRNA. J. Control. Release *304*, 65–74.

59. Blakney, A.K., Yilmaz, G., McKay, P.F., Becer, C.R., and Shattock, R.J. (2018). One size does not fit all: the effect of chain length and charge density of poly(ethylene imine) based copolymers on delivery of pDNA, mRNA, and RepRNA polyplexes. Biomacromolecules *19*, 2870–2879.

60. Badamchi-Zadeh, A., McKay, P.F., Holland, M.J., Paes, W., Brzozowski, A., Lacey, C., Follmann, F., Tregoning, J.S., and Shattock, R.J. (2015). Intramuscular immunisation with chlamydial proteins induces chlamydia trachomatis specific ocular antibodies. PLoS ONE *10*, e0141209.